IEEE Access
Multidisciplinary | Rapid Review | Open Access Journal

Received 3 August 2023, accepted 18 August 2023, date of publication 23 August 2023, date of current version 30 August 2023.

Digital Object Identifier 10.1109/ACCESS.2023.3308043

RESEARCH ARTICLE

Dual Active Bridge Converter With Variable Transformer for Wide Voltage and Wide Load Range Operation

CAMILO SUAREZ BUITRAGO, DIEGO BERNAL COBALEDA, (Student Member, IEEE), AND WILMAR MARTINEZ, (Senior Member, IEEE)
Department of Electrical Engineering (ESAT), KU Leuven, 3590 Diepenbeek, Belgium
Corresponding author: Camilo Suarez Buitrago (camilo.suarez@kuleuven.be)

This work was supported in part by the Frame of the European Center for Power Electronics (ECPE) Joint Research Program.

ABSTRACT This study explores the use of a magnetically controlled transformer within a dual active bridge (DAB) converter. This novel approach introduces a new degree of freedom to the control of the topology through the variation of the equivalent turns ratio of its high-frequency transformer. By adjusting the turns ratio, the converter maintains a primary referred DC voltage gain of one, regardless of varying input/output voltages. This theoretical approach represents the simplest solution to achieve minimum effective currents and enables zero voltage switching (ZVS) under light-load conditions, particularly for unmatched voltage scenarios. This paper provides a comprehensive analysis of the converter's currents, output power, efficiency, and their relationship with the magnetic flux density conditions in the transformer. Furthermore, the trade-off between the total turns ratio variation and the circulating currents in the converter is described in detail. Additionally, considering the specific characteristics of this controllable magnetic device, a straightforward modulation strategy to minimize the effective currents under wide output voltage variations is introduced. An experimental prototype with an input voltage of 100 V and a rated power of 1.2 kW presents a minimum efficiency of 90% under light-load conditions (5% of the maximum load), considering output voltage variations ranging from 130 V to 180 V.

INDEX TERMS Controllable magnetic devices, DAB, variable transformer, ZVS.

NOMENCLATURE

V_1	Input voltage.
V_2	Output voltage.
v_{ac1}	AC voltage generated by the input full bridge.
v_{ac2}	AC voltage generated by the output full bridge.
n	Transformer turns ratio.
f_s	Switching frequency.
T	Switching period.
α	Phase shift angle between v_{ac1} and v_{ac2}.
P_2	DAB average output power.
L	DAB converter series inductance.
L_m	DAB transformer magnetzing inductance.
L_k	DAB transformer leakage inductance.
d	Primary referred DC-voltage gain of the DAB.
w_p	Variable transformer primary winding.
w_s	Variable transformer secondary winding.
N_p	Number of turns of the primary winding.
w_{s1}	Variable transformer secondary winding part a.
N_{s1}	Number of turns of secondary winding part a.
w_{s2}	Variable transformer secondary winding part b.
N_{s2}	Number of turns of secondary winding part b.
$w_{c_{1,2}}$	Variable transformer control winding.
N_c	Number of turns of the control winding.
$\Re v_U$	Variable reluctance.
L_{R_v}	$\Re v_U$ associated inductance.
I_c	Control current.
ϕ_{DC}	Control DC magnetic flux.
$\Re_C$	Fixed reluctance.

The associate editor coordinating the review of this manuscript and approving it for publication was Nagesh Prabhu.

$\Re_{gC}$	Air-gap reluctance.
$L_{\Re_1}$	$\Re_c + \Re_{gc}$ associated inductance.
ϕ_{AC_1}	AC magnetic flux generated at w_p.
ϕ_{AC_2}	AC magnetic flux generated at w_{s2}.
ϕ_{AC_3}	AC magnetic flux through $\Re v_u$.
L_a	Transformer's equivalent series inductance.
L_b	Transformer's equivalent parallel inductance.
n_{eq}	Equivalent turns ratio.
i_1	Transformer's primary current.
i_2	Transformer's secondary current.
i_{Lb}	Transformer's parallel inductance current.
$I_{1_{RMS}}$	i_1 RMS value.
$I_{2_{RMS}}$	i_2 RMS value.
C_{oss}	Switching device output capacitance.
N_{sr}	Turns ratio of the secondary winding.
K	Parallel-series inductance ratio.
G	Equivalent turns ratio gain.
L_r	Equivalent series inductance total variation.
P_{2VT}	DAB average output power with variable transformer.
B_{ACc_x}	AC magnetic flux density in the core-set 'x'.
$B_{ACc_{x_{pk}}}$	AC magnetic peak flux density at the core-set 'x'.
$v_{w_{s1}}$	Voltage in the secondary winding w_{s1}.
$v_{w_{s2}}$	Voltage in the secondary winding w_{s2}.
A_c	Magnetic core effective area.
V_c	Control voltage source.
R_c	Voltage source series resistance.
$I_{T_{RMS}}$	Sum of the currents $I_{1_{RMS}}$ and $I_{2_{RMS}}$.
η	Efficiency.
DAB	Dual Active Bridge.
ZVS	Zero Voltage Switching.
CPM	Conventional Phase-shift Modulation.
DPS	Dual Phase-Shift Modulation.
TPS	Triple Phase-Shift Modulation.
VT	Variable Transformer.
DUT	Device Under Test.
FEA	Finite Element Analysis.

I. INTRODUCTION

The dual active bridge (DAB) converter, first introduced in [1] and depicted in Fig. 1, offers a variety of advantages, such as high efficiency potential, high power density, bidirectional power flow, galvanic isolation, low electromagnetic interference (EMI), and flexibility. Consequently, it has become a popular choice for various applications, including renewable energy systems, electric vehicles, and data centers.

When the DAB is operated under conventional phase-shift modulation (CPM) and matched voltage conditions ($V_1 \approx V_2/n$), it achieves zero voltage switching (ZVS) in both bridges, maintaining high efficiency under a wide range of load conditions, as shown in Fig. 2. However, as discussed in [2], for $V_1 \ll V_2/n$ or $V_1 \gg V_2/n$ high effective currents and hard commutation in the switching elements arise,

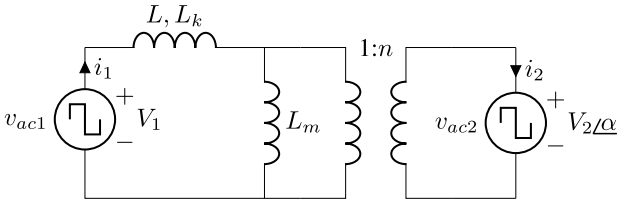

FIGURE 1. DAB converter equivalent circuit representation.

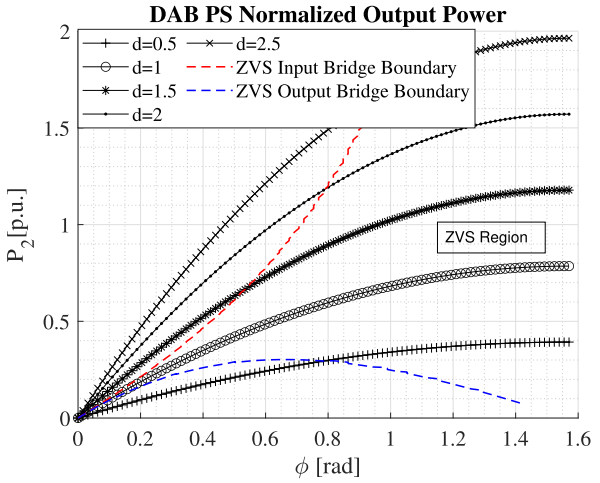

FIGURE 2. ZVS region in a DAB converter under CMP modulation.

particularly for low power levels, affecting the overall performance of the converter.

The regulation of the DAB-CPM output power, defined by equation (1) as established in [3], relies on the shift angle α between the bridge voltages v_{ac1} and v_{ac2}. Although the switching frequency f_s can be utilized for this purpose, large variations in this parameter are avoided, and it is employed mainly as complementary variable [4]. However, the control of these two elements alone is often insufficient to achieve high efficiency under wide load and voltage conditions.

$$P_2 = \frac{V_1^2 d\alpha}{2\pi f_s L}\left(1 - \frac{\alpha}{\pi}\right) \tag{1}$$

where

$$d = \frac{V_2}{nV_1} \tag{2}$$

To overcome this challenge, sophisticated modulation techniques such as dual-phase-shift (DPS) and triple-phase-shift (TPS) have been developed, leading to notable improvements [5], [6], [7], [8], [9], [10], [11], [12], [13]. Nonetheless, due to the analytical and implementation complexity associated with these techniques, their widespread adoption has been limited. Therefore, ongoing research is currently focused on developing simplified variants that reduce the computational resources required, aiming to promote their practical implementation. Additionally, these research efforts aim to tackle other issues, including the discontinuous

transition of the modulation parameters between the different power modes and reducing the reliance on large lookup tables [14], [15], [16], [17].

In contrast to sole control over the switching elements, the authors in [18] propose the use of a variable inductor in series with the high-frequency transformer of the converter, allowing a reduction of the effective currents under light-load conditions by an increment in the converter's inductance L. Similar results were obtained in [19] by the modulation of a coupled series inductance in an input-series output-parallel DAB. However, none of these solutions considered wide-voltage operating conditions in the converter.

A simple approach to address this problem is the use of re-configurable transformers, as presented in [20] and [21]. However, the dynamic response of the employed tap-changer mechanism remains a major concern. Nevertheless, the use of a variable transformer (VT) in a DAB converter capable of maintaining $d \approx 1$ for large variations of V_2 and P_2, would overcome some limitations of the topology.

In this context, the magnetically controlled transformer introduced in [22] is a suitable alternative. Unlike the tap-changer solution, the change in the equivalent turns ratio is continuous and is given by the control of the transformer's equivalent series and parallel inductance by means of a DC current. The variation of its series inductance allows for an improvement in the converter efficiency under light-loads, whereas matched voltage conditions derived from the control of the equivalent turns ratio result in minimum effective currents and ZVS.

The voltage matching range of this VT is inversely proportional to its parallel inductance, which presents one of the trade-offs of the solution. Nevertheless, the use of loosely coupled transformers is known to extend the ZVS region of the DAB converter while considering the parasitic capacitance of the switches [15], [23], [24].

As such, this paper provides a comprehensive analysis of the utilization of this magnetically controlled transformer within a DAB converter. The study begins by introducing the fundamental aspects of the chosen VT and a brief description of the device under test (DUT), including its parameter characterization under small-signal conditions. Subsequently, in the third section, the impact of the variations in the transformer's inductances on the DAB effective currents and the ZVS region is examined. This section also provides insights into the integration of a VT on a DAB converter and its trade-offs. The fourth section discusses the necessary magnetic flux density conditions for the proper operation of the VT, along with the converter's power and current expressions, and the derivation of its extended ZVS region. In addition, a modulation strategy is proposed to minimize the effective currents of the converter. The fifth section presents experimental validation of the analysis, including the transformer re-characterization under the selected operating conditions, average power measurements, proposed modulation strategy results, and converter efficiency. Finally, the conclusions of the study are summarized, highlighting the potential benefits of utilizing a VT to achieve a wide-voltage range DAB converter.

II. THE VARIABLE TRANSFORMER

The VT employed in this study is a magnetic device having controllable parameters. This is achieved by applying DC current to an auxiliary winding in the structure. The induced DC magnetic flux shifts the operating point in the B-H curve of the core's material towards its non-linear region, causing a change in its permeability. Consequently, a variation in the transformer's inductances, equivalent to a change of its effective turns ratio, is achieved.

A. EMPLOYED STRUCTURE

[22, Fig. 3] shows the selected VT structure, it consists of three U-U ferrite core sets and five windings, in which winding w_p, with N_p turns, is tightly coupled to winding w_{s1}, which has N_{s1} turns, and loosely coupled to winding w_{s2}, comprising N_{s2} turns. Nonetheless, this coupling factor can be modified by injecting DC current into the windings $w_{c1,2}$, changing the transformer's equivalent turns ratio between the primary winding, w_p, and the secondary winding (constituted by the series connection of w_{s1} and w_{s2}). Furthermore, the control windings $w_{c1,2}$, with N_c turns, are connected in anti-series and are ideally decoupled from the remaining transformer's windings.

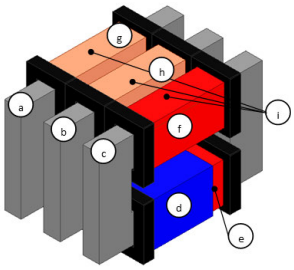

Part	Description
a,b,c	core sets # a,b,c
d	primary winding (w_p)
e,f	secondary winding ($w_{s1,2}$)
g,h	control/ aux. windings ($w_{c1,2}$)
i	air-gap

FIGURE 3. VT description.

B. EQUIVALENT MAGNETIC AND ELECTRIC MODELS

Fig. 4 depicts the AC equivalent magnetic and electric circuits of the VT. In this representation, the DC magnetic flux generated by the current of the control windings, ϕ_{DC}, modifies the reluctance of the core sets a and b, represented by $\Re_{v_U}$. Consequently, its dual element $L_{\Re_v}$, varies as a function of the control DC current I_c. Furthermore, the reluctance of the core set c and its air gap, $\Re_C$ and $\Re_{g_C}$ are not affected by the control flux, resulting in a fixed value for $L_{\Re_1}$. Nevertheless, the models are accurate only for $\phi_{DC} \gg \phi_{AC3}$. This condition allows neglecting the induced voltage on the auxiliary windings and the oscillations on $\Re_{v_U}$ owing to the flux's variations through the transformer primary and secondary windings, ϕ_{AC1} and ϕ_{AC2}. For a detailed analysis, modelling and characterization procedure of the VT, refer to [22].

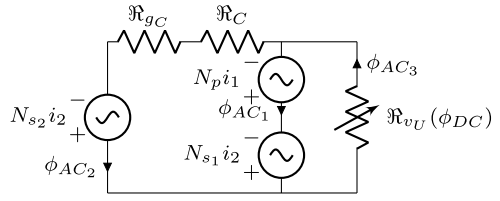

(a) AC magnetic equivalent circuit

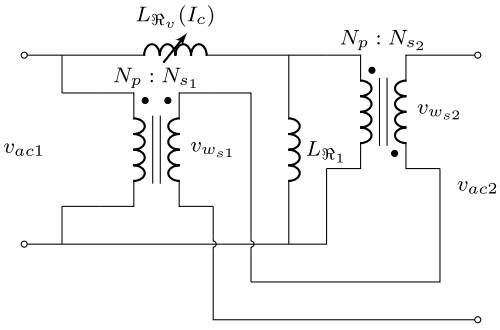

(b) electric circuit representation

FIGURE 4. VT small-signal magnetic and electric circuit representation.

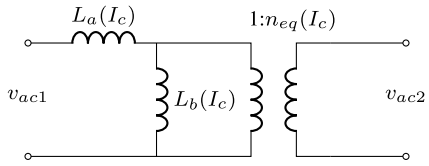

FIGURE 5. VT electrical circuit - cantilever representation.

Although the VT's circuit representation in Fig. 4b is precise, the cantilever model in Fig. 5, simplifies the analysis when the device is integrated into a DAB converter, enabling a direct correspondence between the VT's parameters, L_a, L_b and n_{eq} and the DAB's L, L_m and n. Therefore, the power, current and ZVS region of the DAB+VT converter can be easily extrapolated.

C. DUT

Fig. 6 displays the DUT, its specifications, and its parameter characterization under small-signal conditions. Furthermore, Fig. 6c shows how the equivalent series inductance L_a, the parallel inductance L_b, and the equivalent turns ratio n_{eq} decrease as the control current I_c increases.

More precisely, L_a, L_b and n_{eq} exhibit a 43%, 55% and 28% drop respectively. As shown, the equivalent turns ratio of the transformer varies between 1.89 and 1.38 for a control current between 0 A and 5 A. Likewise, the series inductance decreases from 44.4 μH to 25.4 μH and the parallel inductance from 564 μH to 212 μH.

Furthermore, the rate of change of the transformer inductances differs, causing variations in the parallel series ratio L_b/L_a, which are not appreciated when plotted individually. To fully recognise these variations, the relative changes of the parameters are depicted in Fig. 6d. As shown, L_b/L_a is not constant and reaches a minimum value of 7.4 between the initial and final states of VT.

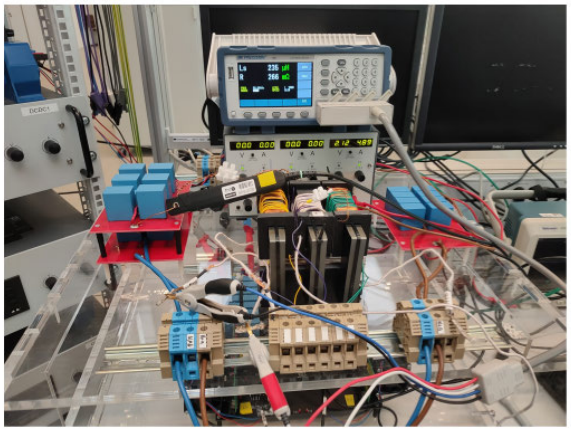

(a) DUT under test

Core Reference	U93/76/16
Material	3C94
Air-gap	120 μm
# of turns N_p, N_{s_1}, N_{s_2},N_c	10 , 20, 10, 50

(b) DUT specs

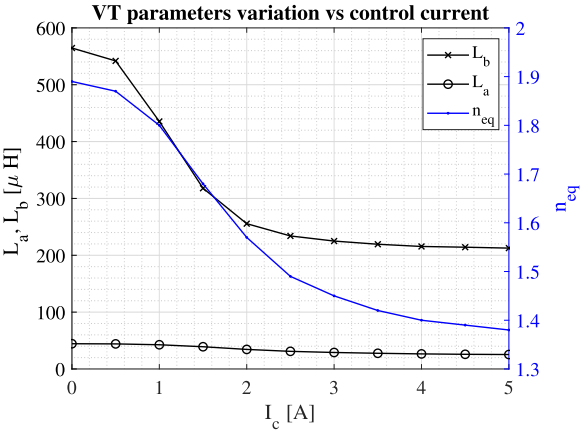

(c) VT's parameters variation

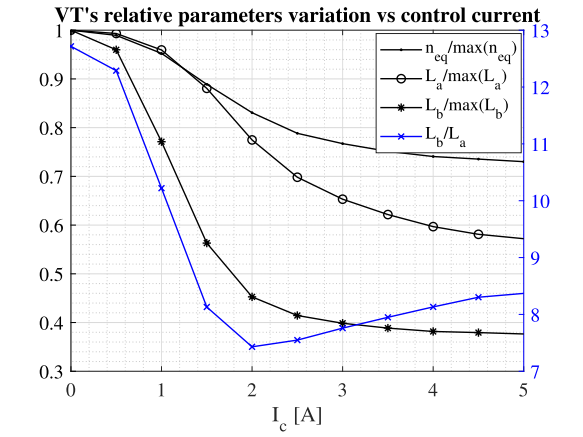

(d) Relative VT parameters variation

FIGURE 6. DUT specifications and small-signal characterization (Open-short circuit test).

As observed, the flow of DC current through the control winding induces changes in the transformer's coupling factor. Consequently, the equivalent turns ratio can be

modified, allowing matched voltage conditions in a DAB converter within a range of the output-input voltage ratio of $1.38 < V_2/V_1 < 1.89$.

Therefore, setting the parameter d close to one through a variation of n_{eq}, it is possible to improve the converter efficiency under varying voltage conditions and light loads. This improvement is achieved by the reduction of the converter's effective currents and switching losses. Notably, the use of the DUT results in negligible increases in circulating currents due to the relatively high minimum ratio between L_b/L_a (> 7.5). Further details are provided in the following section.

III. VT'S PARAMETERS VARIATION IMPACT ANALYSIS ON THE DAB CONVERTER

In this section, a three-step analysis is conducted to examine the implications of the VT's parameter variations on the DAB performance. First, the effect of varying the transformer's magnetizing inductance, L_m, under different voltage ratios is assessed. Next, a similar analysis is performed in terms of the leakage inductance, L_k. Finally, the VT's parameter variations as a whole are discussed to obtain a better understanding of the proposed solution trade-offs.

A. VARIATION OF THE MAGNETIZING INDUCTANCE

Typically, the magnetizing inductance in a DAB transformer is sufficiently high to be ignored. However, for values of L_m close to L_k, the effective currents of the transformer might significantly increase. To evaluate this condition, the normalised equivalent DAB circuit in Fig. 7a is analysed. The effective currents of the transformer $I_{1,2RMS}$ under matched voltage conditions are plotted as a function of the output power P_2 while varying L_m, see Figs. 7b-7c.

As this scenario illustrates, for $V_1 \approx V_2/n$, the circulating currents are not particularly high, even for low values of the magnetizing inductance, as low as $L_m/L_k = 5$. However, for unmatched voltage conditions ($V_1 \ll V_2/n$ or $V_1 \gg V_2/n$), the effective currents increase substantially, despite high L_m values of $100L_k$, as shown in Fig. 8.

By comparing the effective currents of the DAB transformer in Figs. 7b, 7c and Fig. 8b under light load conditions, it becomes evident that maintaining $V_1 \approx V_2/n$ proves to be more advantageous than achieving a high parallel-series inductance ratio in the transformer. This is relevant in the VT analysis where a significant change in the equivalent turns ratio implies a pronounced drop in the parameter L_b/L_a, becoming one of its main trade-offs.

However, as described by the authors in [23], [24], [25], [26], and [27], a reduction in the magnetising inductance of a DAB's transformer can lead to an extension of the ZVS region. As shown in Fig. 9, the output bridge ZVS boundary of the circuit in Fig. 7 shifts to the left as L_m decreases. Thus, a reduced selection of the parallel-series inductance ratio can improve the converter's performance, even under no-load condition. Nevertheless, a precise definition of the ZVS region requires consideration of the charge-based conditions detailed in [28].

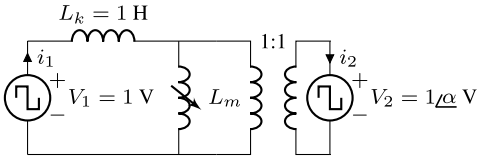

(a) DAB having variable L_m under matched voltage condition

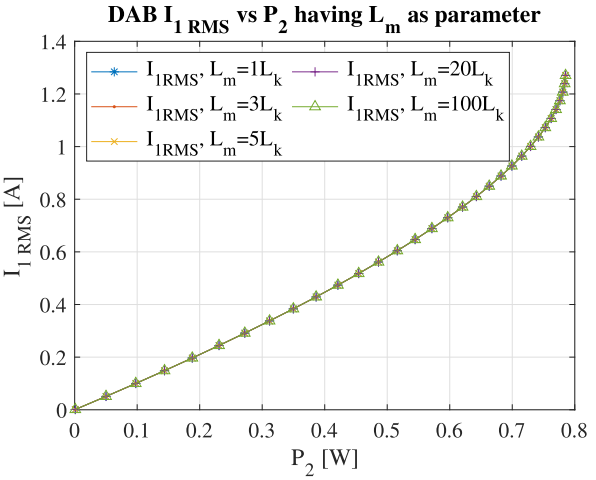

(b) I_{1RMS} vs P_2

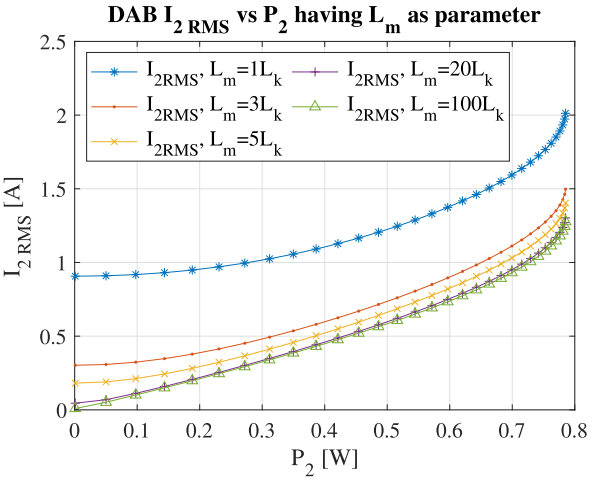

(c) I_{2RMS} vs P_2

FIGURE 7. DAB transformer's effective currents having L_m as parameter under-matched voltage conditions.

B. VARIATION OF THE SERIES/LEAKAGE INDUCTANCE

The transformer's leakage inductance partly regulates the DAB converter output power, as defined by equation (1). Under unmatched voltage conditions, reducing the value of L_k increases P_2 along with the circulating currents, particularly under light-load conditions. This is illustrated in Fig. 10, where decreasing L_k by half doubles the effective currents for $V_1 \neq V_2/n$, represented by the color lines, and extends the power range by a factor of two when compared to the case shown in Fig. 8. Moreover, this causes the ZVS region to narrow at low power levels, as shown in Fig. 10c.

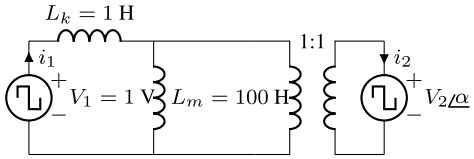

(a) DAB converter having $L_m \gg L_k$ under unmatched voltage conditions

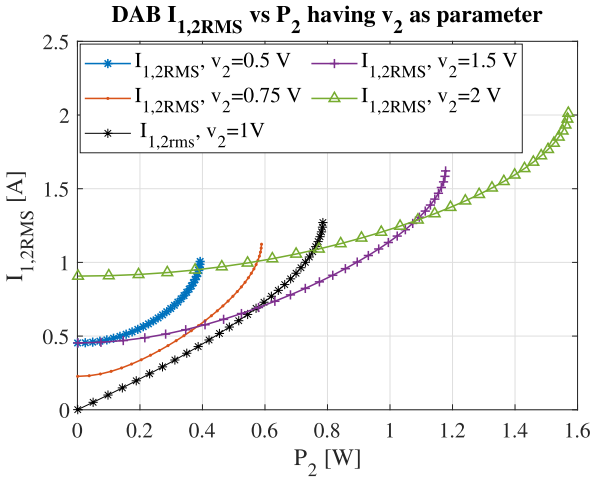

(b) $I_{1,2RMS}$ vs P_2

FIGURE 8. DAB transformer's effective currents having V_2 as parameter and high magnetizing inductance.

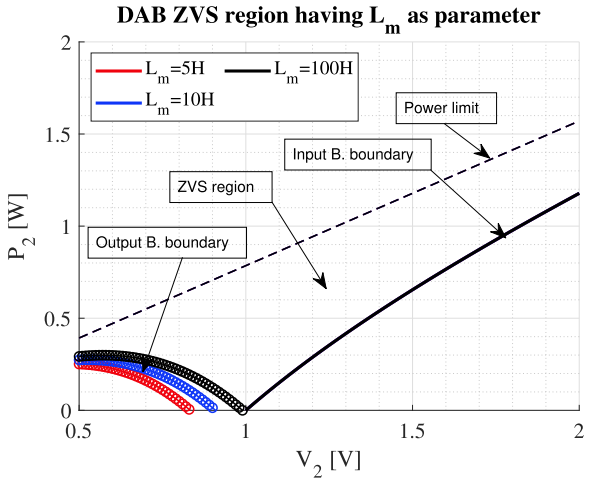

FIGURE 9. DAB current-based ZVS region having L_m as parameter.

Conversely, under matched voltage conditions, $V_1 \approx V_2/n$, reducing L_k results in a quasi-linear behavior of the effective current across a broader range of power, with minimum values in this region (see Fig. 10b, black line). However, when this behaviour no longer holds at $P_2 > 1.08$ W, the operation in boost mode ($V_1 < V_2/n$), represented by the green and purple lines in Fig. 10b, results in lower values of $I_{1,2RMS}$.

In terms of soft commutation, the current-based conditions to achieve ZVS for both bridges are satisfied for virtually all power levels.

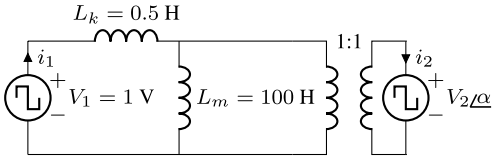

(a) DAB converter with reduced L_k

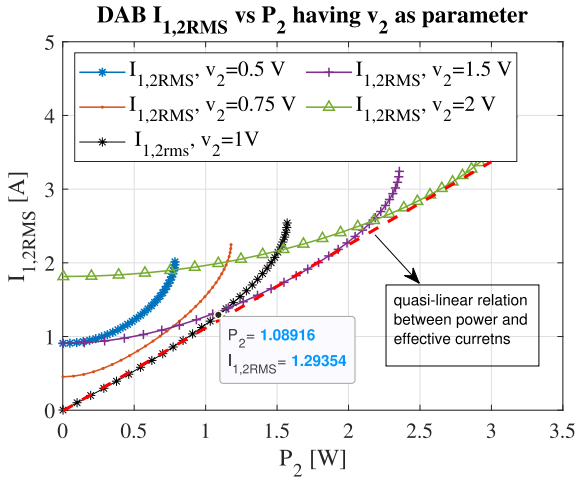

(b) $I_{1,2RMS}$ vs P_2 for $L_k = 0.5$ H having V_2 as parameter

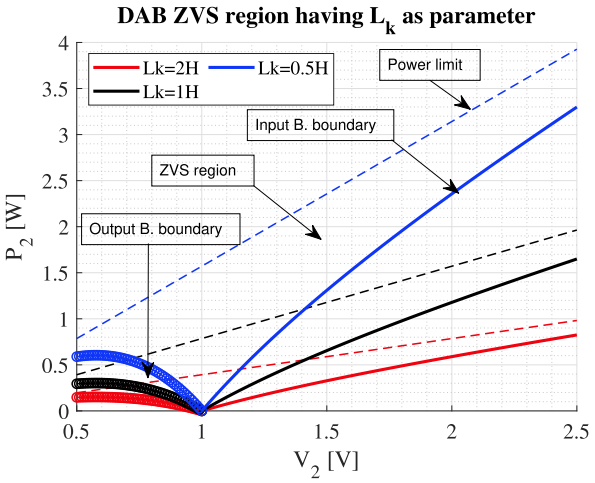

(c) ZVS region having L_k as parameter

FIGURE 10. DAB effective currents for a $L_k = 0.5$ H and current-based ZVS region having L_k as parameter.

In general, a gradual reduction of L_k as the converter's load increases enables the achievement of minimum effective currents associated with the particular input-output voltage conditions while extending the ZVS region, as explained in [18]. Consequently, a significant variation of L_k leads to an efficient wide-load operation capability. However, it is essential to ensure matched voltage conditions for light loads.

C. VT SOLUTION TRADE-OFFS

As mentioned before and depicted in Fig. 6c, the variation of the VT's equivalent turns ratio n_{eq} (and its capability to match V_2) implies a decrease in the structure's parallel and

series inductances L_a and L_b. Although a reduction in these parameters might represent an improvement in the converter's performance under light-load and wide-voltage range conditions; it can also significantly increase the circulating currents and conduction losses. To mitigate this problem, the VT's secondary turns ratio, N_{sr}, must be selected to guarantee a minimum predefined parallel-series inductance ratio K that achieves the required turns ratio gain, G, given by (3) (4) and (5) respectively.

$$N_{sr} = \frac{N_{s2}}{N_{s1}} \tag{3}$$

$$G = \frac{n_{eq}|_{I_c=0}}{n_{eq}|_{I_c=I_{cmax}}} \tag{4}$$

$$K = min\left(\frac{L_b(I_c)}{L_a(I_c)}\right) \tag{5}$$

Fig. 11 illustrates the relation between K, G, and N_{sr} for the DUT, consistent with the expressions derived in [22]. As shown, the gain of the VT's turns ratio can be increased by adjusting N_{sr}, allowing it to change its value from 1.37 to a maximum of 1.46. However, this would result in a substantial reduction of K, decreasing from a minimum value of 7.4 to 25, leading to a significant increase in the transformer's secondary effective current, as shown in Fig. 7c. Moreover, the series inductance total variation (L_r in equation (6)) would be reduced, limiting the extension of the quasi-linear relation region between the output power and the transformer effective currents.

$$L_r = \frac{L_a|_{I_c=0}}{L_a|_{I_c=I_{cmax}}} \tag{6}$$

This particular implementation of the VT presents a relatively limited gain capability, which can pose challenges to fully understand the trade-offs among the parameters. This can be attributed to the minor overall variation of the controllable reluctance $\Re_{v_U}$, mainly caused by the influence of the transformer stray reluctance. Thus, the parameter G barely undergoes significant changes, as depicted in Fig.11b.

Nonetheless, it is possible to substantially enhance the turns ratio gain, as described in [22], by employing modified core arrangements that increase the coupling among the VT windings. This results in a higher value of K without altering the ratio between the turns of the secondary winding. Despite this improvement, the inherent trade-off of the structure remains: the variation of the transformer's turns ratio gain, G, is inversely proportional to both K and L_r.

IV. DAB+VT CONVERTER ANALYSIS

The power and current expressions used to analyze a regular DAB converter can also be applied to the DAB+VT. However, to ensure the validity of this approach, the parameters L_a, L_b and n_{eq} should only vary against the control current I_c. Consequently, the fluctuation of these parameters due to the transfomer AC magnetic fluxes must be negligible. Considering this, the small-signal representation of the DAB+VT is

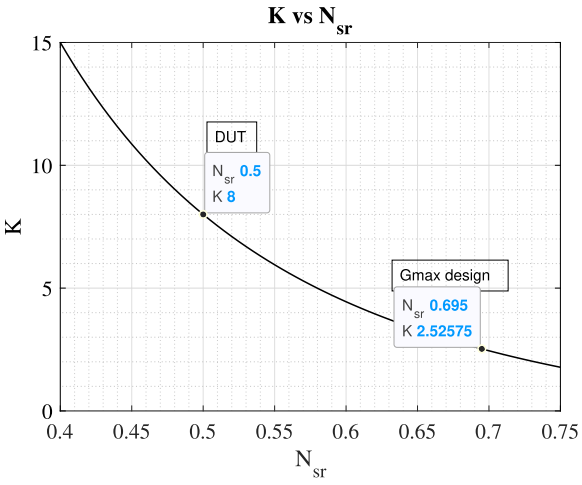

(a) K vs N_{sr}

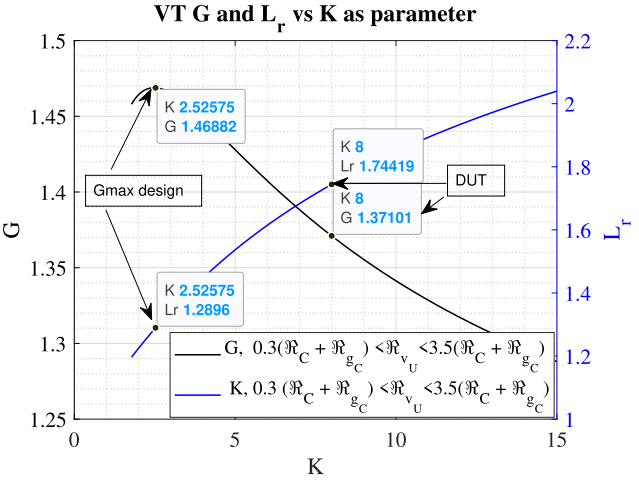

(b) G and L_r vs K

FIGURE 11. DUT's turns ratio gain G and series inductance total variation L_r vs minimum parallel-series inductance ratio K.

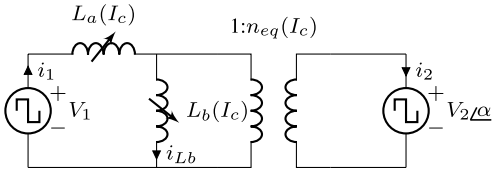

FIGURE 12. DAB+VT small signal equivalent circuit representation.

depicted in Fig. 12, and its power expression is given by (7), directly derived from (1).

$$P_{2VT} = \frac{V_1 V_2 \alpha}{2\pi f_s L_a(I_c) n_{eq}(I_c)}\left(1 - \frac{\alpha}{\pi}\right) \tag{7}$$

A. DAB+VT MAGNETIC FLUX DENSITY AND TRANSFORMER'S SMALL-SIGNAL OPERATION CONSIDERATIONS

To determine the AC flux densities in the VT's cores ($B_{AC_{Ca-c}}$), the transformer's windings voltage are defined and given by the equations (8)-(10), according to the VT's

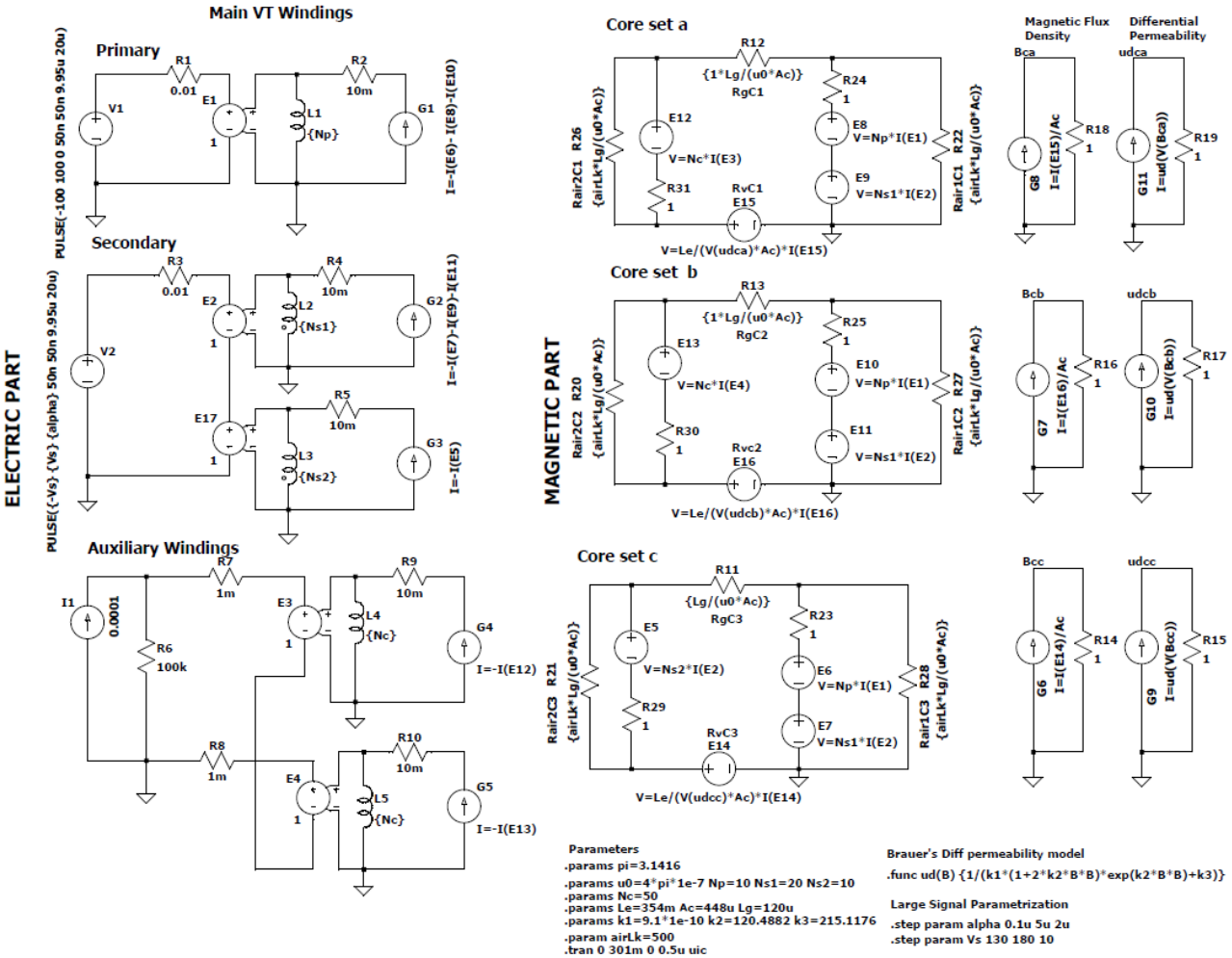

FIGURE 13. DAB+VT spice model.

magnetic and electric circuit representation shown in Fig. 4.

$$v_{w_{s1}} = \frac{N_{s1} v_{ac1}}{N_p} \tag{8}$$

$$v_{ac1} = N_p \frac{d(\phi_{AC_1})}{dt} \tag{9}$$

$$v_{w_{s2}} = v_{ac2} - v_{w_{s1}} = N_{s2} \frac{d(\phi_{AC_2})}{dt} \tag{10}$$

where

$$\phi_{AC_2} = A_c B_{AC_{Cc}} \tag{11}$$

$$\phi_{AC_3} = \phi_{AC_1} + \phi_{AC_2} \tag{12}$$

$$\phi_{AC_{3(I_c=0)}} = 2A_c B_{AC_{Ca}} \tag{13}$$

$$B_{AC_{Ca}} \approx B_{AC_{Cb}} \tag{14}$$

Thus, considering the voltage waveforms of the DAB under CPM, the core peak flux densities of the VT can be derived as follows:

$$B_{AC_{Capk}} = \frac{1}{2A_c f_s}\left(\left(\frac{\alpha}{2\pi} - \frac{1}{4}\right)\left(1 - \frac{N_{s1}}{N_{s2}}\right)\frac{V_1}{N_p} - \frac{V_2}{4N_{s2}}\right), \quad \frac{V_2}{V_1} \geq \frac{N_{s1} - N_{s2}}{N_p} \tag{15}$$

$$B_{AC_{Ccpk}} = \frac{1}{2N_{s2}A_c f_s}\left(\left(\frac{\alpha}{\pi} - \frac{1}{2}\right)V_2 + \frac{V_1 N_{s1}}{2N_p}\right), \quad \frac{V_2}{V_1} \leq \frac{N_{s1}}{N_p} \tag{16}$$

To ensure the operation of the VT at small-signal level, the AC magnetic peak flux density of the cores subject to pre-magnetization ($B_{AC_{Ca,bpk}}$) should not exceed 50 mT, in accordance with the considerations of the authors in [29]. If this condition is not satisfied, simulations are required to determine the converter's operation, with finite element analysis (FEA) being the most precise method. However, conducting FEA simulations requires considerable time and resources. Alternatively, SPICE-based behavioral models can be utilized. Hence, based on the work presented in [30] a

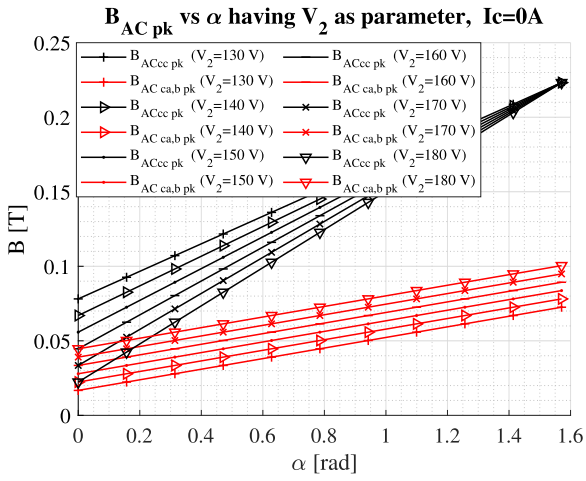

(a) Analytical expression

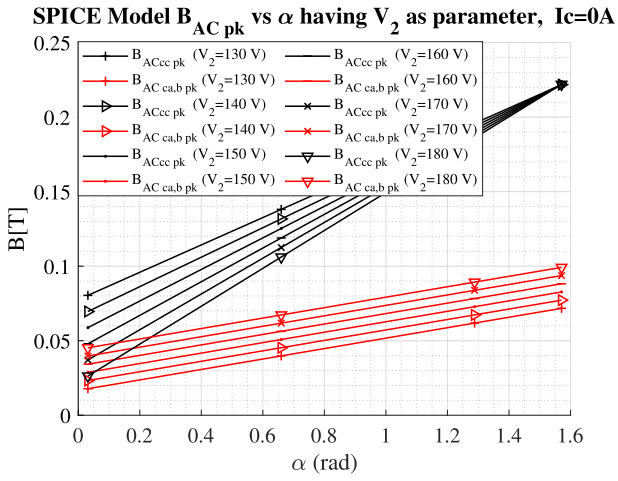

(b) SPICE model

FIGURE 14. VT magnetic core flux densities vs α having V_2 as parameter for $I_c = 0A$: analytical expressions vs simulation results.

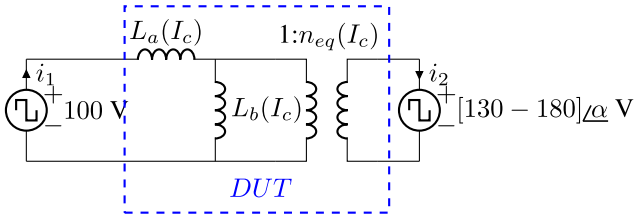

FIGURE 15. DAB+VT experimental voltage conditions ($f_s = 50kHz$).

SPICE model for the DAB using a VT was built as shown in Fig. 13.

A comparison between the flux density at the VT's cores obtained using the analytical expressions (15)-(16) and the SPICE model is depicted in Fig. 14. The selected voltages, $V_1 = 100$ V and 130 V $\leq V_2 \leq 180$ V correspond to those employed in the experimental section of this paper, see Fig.15. As seen, the obtained results validate the conducted analysis, showing a clear correspondence between both cases.

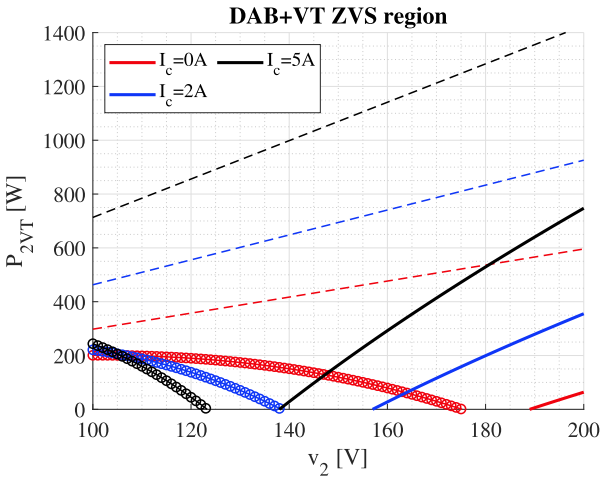

FIGURE 16. DAB+VT ZVS current-based boundary conditions region having I_c as parameter.

When the reluctance of the stray path is disregarded, the fluxes within the transformer cores remain unaffected by the control current I_c. However, even when this element is considered, the maximum flux densities in the VT cores occur at $I_c = 0$ A. Thus, it is necessary to verify the achievement of small-signal conditions for the VT for this particular scenario.

For high magnetic flux variations ($B_{ACCa,bpk} > 50$ mT) the concept of differential permeability, employed to describe the VT's parameters variation, becomes inaccurate. Therefore, the previous models discussed in this paper do not properly describe the non-linear behavior of the resultant transformer currents.

B. DAB+VT CURRENTS AND ZVS REGION

Under small-signal operation, the derivation of the DAB+VT currents values in equations (17)-(18) follows the analysis performed in [3].

$$i_1(0) = \frac{V_1}{2\pi f_s L_a(I_c)}\left(\frac{V_2}{n_{eq}(I_c)}\left(\frac{\pi}{2} - \alpha\right) - \frac{\pi}{2}\right) \tag{17}$$

$$i_1(\alpha) = \frac{V_1}{2\pi f_s L_a(I_c)}\left(\alpha + \frac{\pi}{2}\left(\frac{V_2}{n_{eq}(I_c)} - 1\right)\right) \tag{18}$$

Similarly, the ZVS current-based boundary conditions for the input and output bridges are given by (19) and (20) respectively.

$$i_1(0) \leq 0 \tag{19}$$

$$i_1(\alpha) - i_{Lb}(\alpha) \geq 0 \tag{20}$$

where the current of the parallel inductor i_{Lb}, is derived by inspection from the circuit in Fig. 12.

$$i_{Lb}(\alpha) = -\frac{V_2}{4n_{eq}(I_c) f_s L_b(I_c)} \tag{21}$$

Thus, considering the previous expressions, the ideal turn-on soft-switching region for the DAB+VT converter under

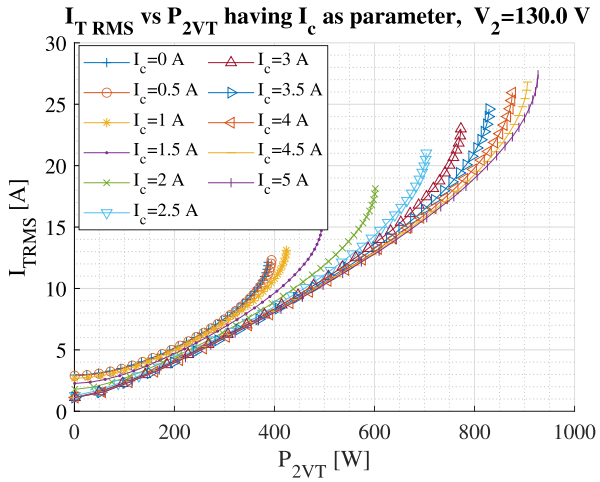

(a) I_{TRMS} vs P_{2VT} at $V_2 = 130$ V

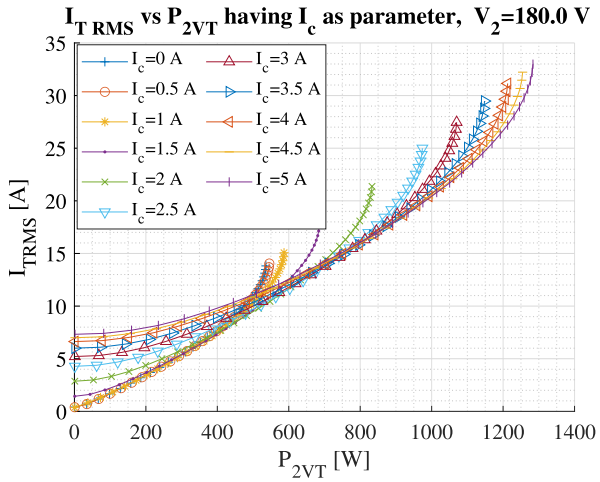

(b) I_{TRMS} vs P_{2VT} at $V_2 = 180$ V

FIGURE 17. Theoretical total transformer effective current I_{TRMS} vs P_{2VT} having I_c as parameter for different V_2 voltages.

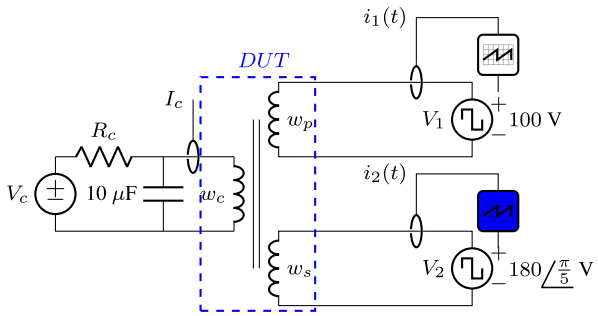

(a) VT's working principle measured signals and voltage source configuration

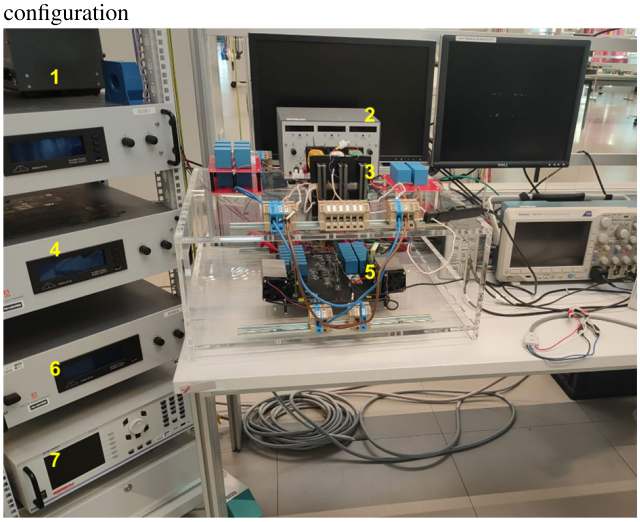

Part	Description
1	μController voltage source: Delta EST 150
2	V_c: Delta EST 150
3	DUT: VT
4	V_1: Delta SM500-CP-90
5	DAB converter (MOSFET:C3M0030090K)
6	V_2: Delta SM500-CP-90
7	Power analyzer: Zimmer LMG 500

(b) Experimental set-up description

FIGURE 18. DAB+VT current measurement schematic and experimental set up.

the aforementioned experimental conditions are illustrated in Fig. 16. As shown, the input and output boundaries shift towards the left with an increase in the control current I_c, which indicates a decrease in the equivalent turn ratio of the VT. Additionally, a drop in the series inductance leads to an increase in the power level, indicated by the dotted lines. Furthermore, the reduction in the parallel-series inductance ratio extends the ZVS region at low power levels.

C. EFFECTIVE CURRENTS AND MINIMIZATION STRATEGY

The modulation strategy proposed in this study aims to minimize the effective currents of the DAB+VT, particularly under wide voltage and light-load conditions. The approach involves assessing the combination of the converter's controllable parameter $L_a n_{eq}(I_c)$, and shift angle α to achieve a specific output power P_{2VT} at a given output voltage V_2. Then, the (I_c, α) pair that minimizes the sum of the VT's effective currents (equation (22)), is registered into the lookup table of the modulation.

$$I_{T_{RMS}} = I_{1_{RMS}} + I_{2_{RMS}} \tag{22}$$

Fig. 17 displays the theoretical values of $I_{T_{RMS}}$ of the DUT for different output bridge voltages, plotted against the DAB+VT output power, with the control current as parameter. As shown in Fig. 17a, at $V_2 = 130$ V, $I_c = 5$ A yields the lowest effective currents and highest power range, owing to the combined effect of a reduction in the series inductance and the equivalent turns ratio. On the other hand, for $V_2 = 180$ V, $I_c = 0$ A leads to a significant reduction in the circulating current at light loads. Moreover, as the load increases, an increment in the control current results into the entry

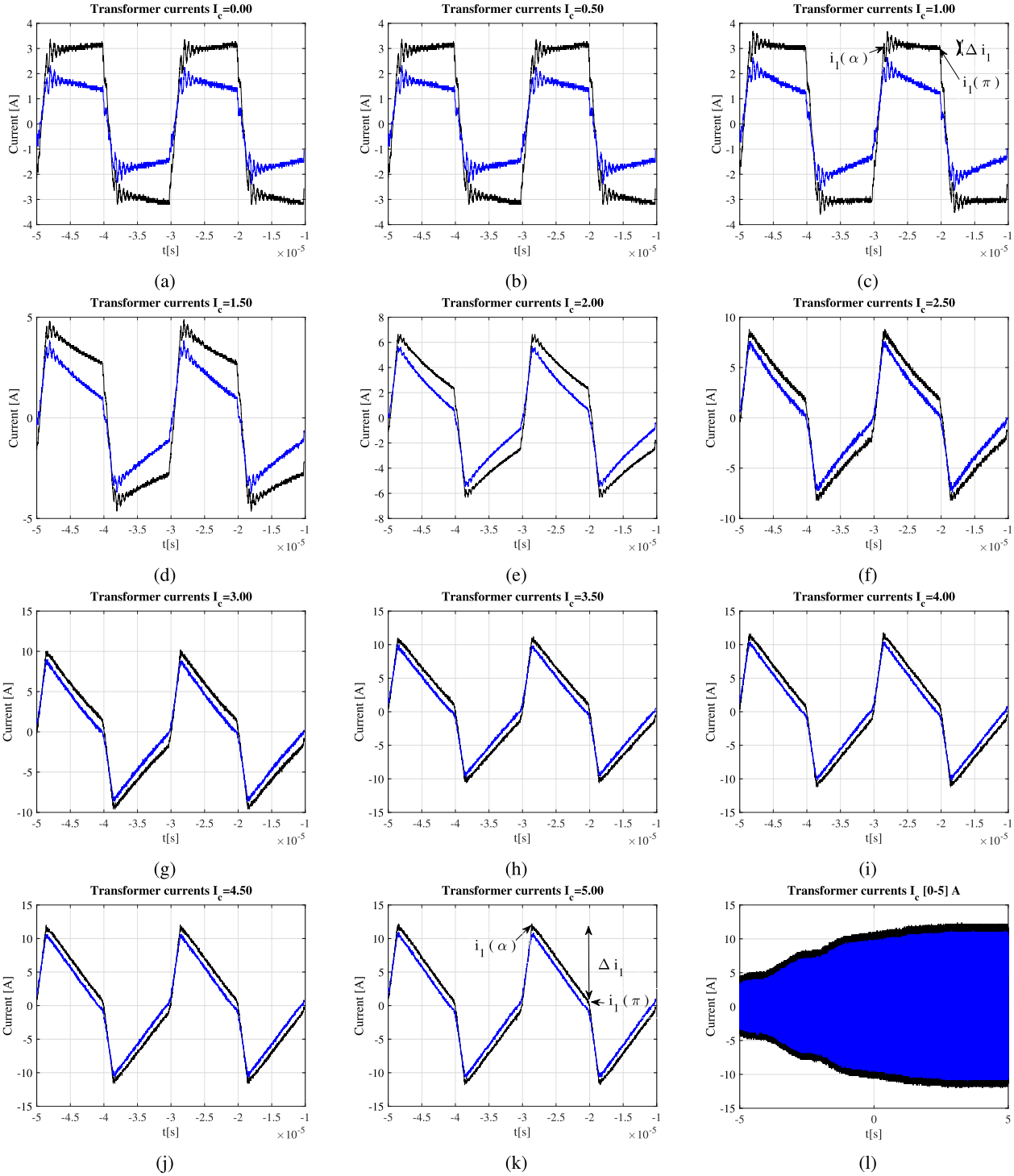

FIGURE 19. VT's experimental currents waveforms following the configuration in Fig.18: (a)-(k) i_1 and i_2 (blue) for control currents (0, 0.5, 1, 1.5, 2, 2.5, 3, 3.5, 4, 4.5, 5) A. (l) Primary and secondary currents (blue) in response to a continuous variation of I_c from 0 to 5 A.

of the converter in boost mode and the maintenance of the quasi-linear relationship between P_{2VT} and $I_{T_{RMS}}$, clearly shown in Fig. 17b.

In line with the analysis presented in Section III, when operating under light-load conditions, adjusting $d \approx 1$ by means of the VT enables a reduction in the circulating currents. Conversely, at heavy-load conditions, irrespective of the primary referred DC-voltage gain, a decrease in the series inductance is desirable. It is important to note that the transition of current values for different voltage conditions is continuous thanks to the ability to continuously adjust the control current as well.

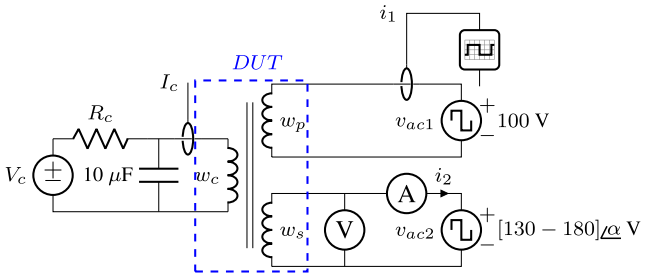

FIGURE 20. Measurement schematic of the DUT's parameter estimation under operating conditions.

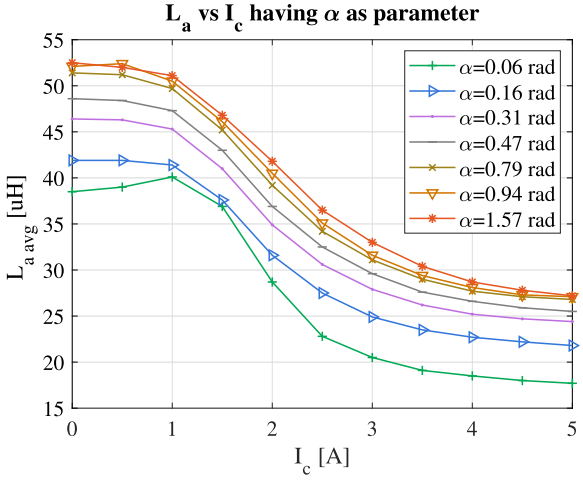

(a) L_a vs I_c having α as paramerter

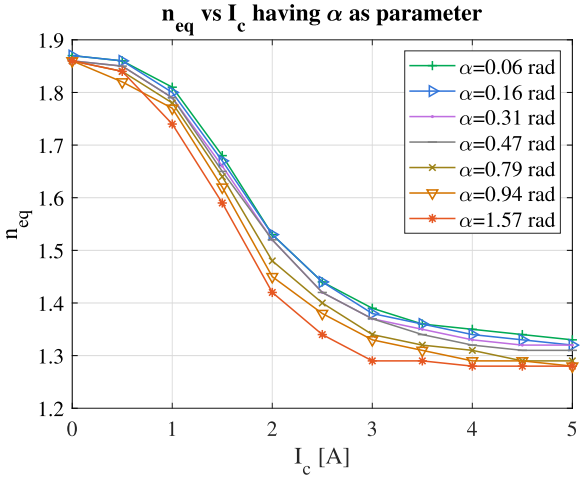

(b) n_{eq} vs I_c having α as parameter

FIGURE 21. VT parameters characterization at converter's operating conditions.

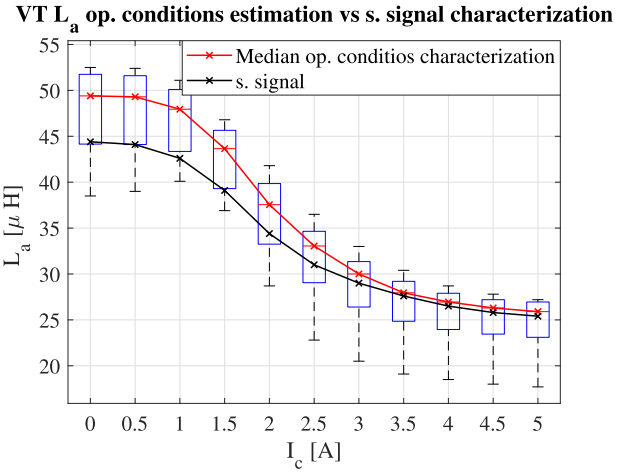

(a) L_a box-plot and small signal characterization

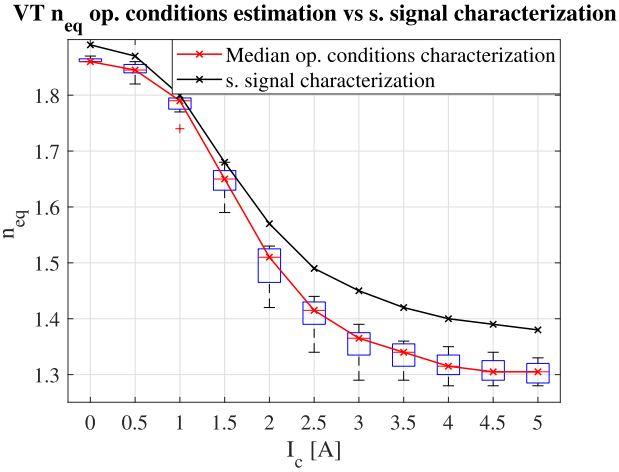

(b) n_{eq} box-plot and small signal characterization

FIGURE 22. VT parameter's comparison according to the characterization procedure.

V. EXPERIMENTAL VALIDATION

A. DAB+VT WORKING PRINCIPLE

The working principle of the DAB+VT converter is verified by inspecting the ratio between the transformer's currents as a function of the control current I_c, following the configuration and experimental DAB set-up shown in Fig. 18. As seen, V_1, V_2, and α are fixed, whereas the control current varies from 0 A to 5 A.

Fig. 19a-19c illustrates the behavior of the transformer's currents for $I_c < 1$ A. In this range, the VT maintains a nearly constant value of $n_{eq} \approx 1.89$, resulting in $V_1 \approx V_2/n_{eq}$. Consequently, the primary current i_1 (shown in black) remains steady during the time interval $\frac{\alpha T}{2\pi} < t < T/2$. For this condition, the current slope is nearly null as the voltage difference at the transformer series inductor is close to zero.

As the control current increases, both i_1 and i_2 increase, leading to higher output power from the converter due to a reduction in L_a. Simultaneously, the amplitude difference between the transformer's currents is reduced, indicating a decrease in n_{eq} (shown in Fig. Fig. 19d-19j). When the final transformer state is reached ($I_c = 5$ A, as depicted in Fig. 19k), both currents have comparable magnitudes, indicating that the equivalent turns ratio is close to one, deriving in a current variation for the same interval, as $V_1 \neq V_2/n_{eq}$.

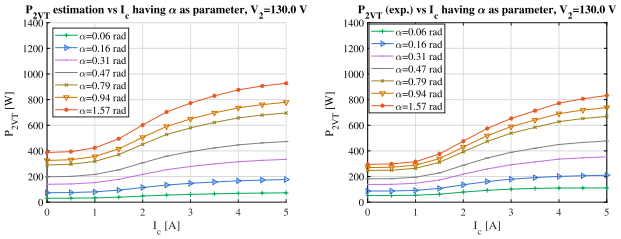

(a) P_{2VT} small signal estimation, $V_2 = 130$ V (b) P_{2VT} measurement, $V_2 = 130$ V

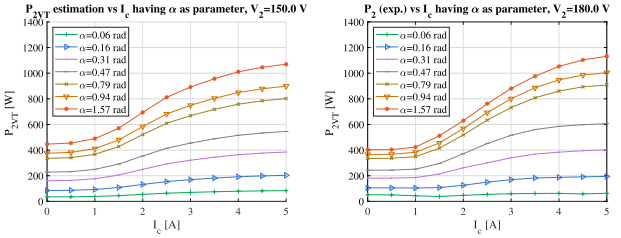

(c) P_{2VT} small signal estimation, $V_2 = 150$ V (d) P_{2VT} measurement, $V_2 = 150$ V

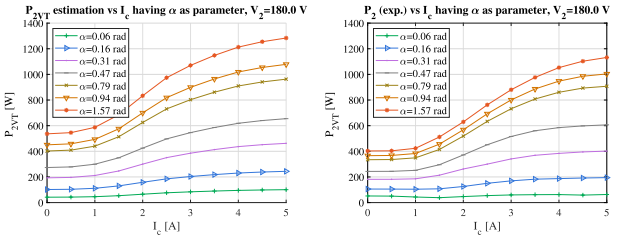

(e) P_{2VT} small signal estimation, $V_2 = 180$ V (f) P_{2VT} measurement, $V_2 = 180$ V

FIGURE 23. DAB+VT average power small-signal estimation vs operating conditions measurements.

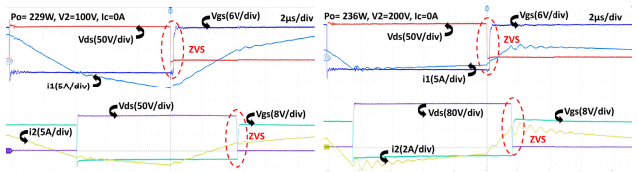

(a) $V_2 = 100$ V, $P_{2VT} = 229$ W (b) $V_2 = 200$ V, $P_{2VT} = 236$ W

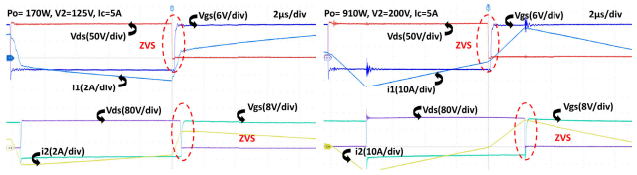

(c) $V_2 = 125$ V, $P_{2VT} = 170$ W (d) $V_2 = 200$ V, $P_{2VT} = 910$ W

FIGURE 24. ZVS waveforms for input (top) and output bridge (bottom) for the theoretical voltage region limits.

Finally, Fig. 19l shows the transition of the transformer's currents for a continuous variation of the control current I_c form 0 A to 5 A. As seen, the increments of the primary and secondary currents are continuous and monotonic during the transformer's states variation.

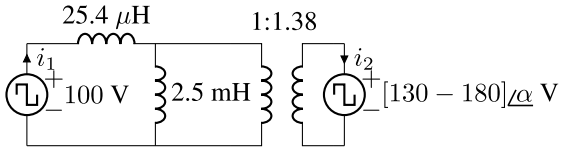

FIGURE 25. Reference DAB converter (DAB REF.).

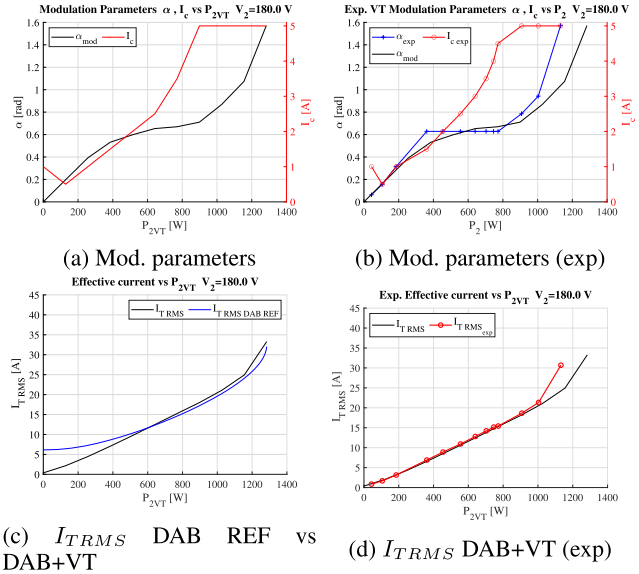

(a) Mod. parameters (b) Mod. parameters (exp)

(c) I_{TRMS} DAB REF vs DAB+VT (d) I_{TRMS} DAB+VT (exp)

FIGURE 26. Modulation parameters and experimental results for $V_2 = 180$ V.

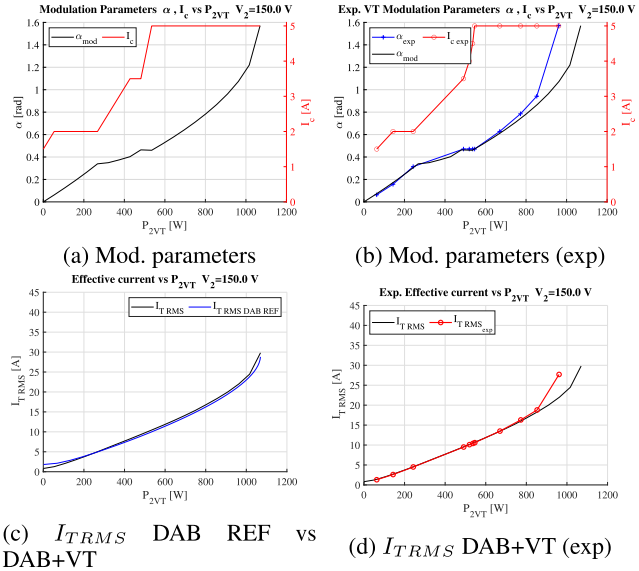

(a) Mod. parameters (b) Mod. parameters (exp)

(c) I_{TRMS} DAB REF vs DAB+VT (d) I_{TRMS} DAB+VT (exp)

FIGURE 27. Modulation parameters and experimental results for $V_2 = 150$ V.

B. VT'S PARAMETER ESTIMATION AT OPERATING CONDITIONS

A re-characterization of the VT is conducted to detect deviations in the parameters presented in Section II resulting from large variations in the flux density of the core, associated

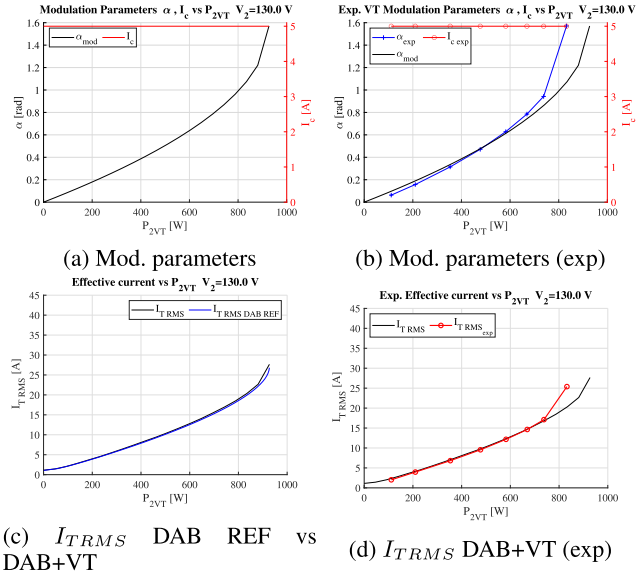

(a) Mod. parameters (b) Mod. parameters (exp)

(c) I_{TRMS} DAB REF vs DAB+VT (d) I_{TRMS} DAB+VT (exp)

FIGURE 28. Modulation parameters and experimental results for $V_2 = 130$ V.

with the converter's specific operating voltage levels. In this context, L_a and n_{eq} are estimated directly from the converter's operation by imposing a trapezoidal current waveform for i_1, concordant with the condition expressed in (23), and measuring the average output power of the converter, as illustrated in Fig. 20. Consequently, by adjusting V_2 to obtain $i_1(\alpha) = i_1(\pi)$ for a given pair (α, I_c), n_{eq} and L_a can be solved from equations (24) and (7), respectively.

$$\Delta i_1 = T\left(\frac{1}{2} - \frac{\alpha}{2\pi}\right)\frac{(V_1 - \frac{V_2}{n_{eq}(I_c)})}{L_a(I_c)} = 0 \tag{23}$$

$$n_{eq}(I_c) = V_2/V_1 \tag{24}$$

It is worth noticing that the condition in (23) is only achieved at $V_1 = \frac{V_2}{n_{eq}(I_c)}$, as derived from the circuit analysis of the DAB converter under CPM in Fig. 15.

As shown in Fig. 21a, L_a is highly dependent on the shift angle α, resulting in a wide variation of this parameter. This behavior is linked to the proportional increment of $B_{AC_{Capk}}$, leading to a larger deviation from the characterization results obtained under small-signal conditions. Additionally, the estimation procedure does not account for the converter's efficiency, causing the losses of the system to be represented by an increase in the value of L_a.

In contrast, there is no direct relation between α and n_{eq}, as illustrated in Fig. 21b. This behavior can be partially attributed to the negligible influence of the converter's efficiency on the parameter estimation.

A statistical comparison between the VT's parameters, considering the converter operating conditions, and the small-signal characterization results is presented in Figs. 22a and 22b.

The observed differences indicate deviations in the estimation of the converter's nominal power, revealing its dependence on the magnetic flux density levels within the transformer's cores.

C. DAB+VT AVERAGE POWER MEASUREMENTS

The converter's output power P_{2VT} was calculated using the transformer's parameters in Section II and compared to the experimental measurements, as shown in Fig. 23. Voltage V_1 was kept constant at 100V while V_2 was set at 130 V, 150 V, and 180 V. For each of these conditions, an I_c sweep was performed with the converter's shift angle α as a parameter.

As seen, increasing the output voltage and shift angle directly contributes to a higher power mismatch, as the AC magnetic flux is proportionate to V_2 and α. Consequently, there is a decrease in the overall power capacity of the converter. However, this limitation can be addressed by restricting the shift angle to values below $\pi/4$. By doing so, the power of the converter remains within the quasi-linear region and limits the flux density of the core, without significantly derating the converter's output power.

The calculated values obtained using the VT small-signal characterization align well with the experimental results, especially for $\alpha < \pi/4$. This correspondence suggests that expression (7) provides a good balance between accuracy and complexity when small-signal conditions are met, as defined in Section IV. Although deviations occur for higher magnetic flux values exceeding 50 mT, resulting in a decrease in the converter's power capacity, the power curves still present the expected trend. Furthermore, the variations to the transformer's equivalent turns ratio are in line with the model.

D. DAB+VT ZVS REGION

Fig. 24 illustrates the current and voltage waveforms associated with achieving zero voltage switching at the input and output bridges of the converter under the output voltage conditions outlined in Fig. 16. The effect of the reduced parallel inductance, L_b, is offset by the MOSFETs' output capacitance, C_{oss}. This implies that non-zero power levels are required to achieve soft commutation [25]. Consequently, to effectively extend the ZVS region by taking advantage of the variation in the equivalent turns ratio, a careful selection of the VT's parameter K, winding capacitance, and MOSFETs characteristics is necessary. Nevertheless, the VT has been shown to be effective in attaining the ZVS current-based conditions stated in [3] under the considered voltage variations.

E. MODULATION RESULTS

The proposed modulation technique for reducing the effective currents of the converter is based on evaluating the power of the converter in all possible scenarios using α and I_c as parameters. The obtained results can be compared to those of a conventional DAB operating in boost mode. To ensure an accurate comparison, the turns ratio and leakage inductance of the reference converter are set equal to the minimum values achieved by the DUT, while a large magnetizing inductance is

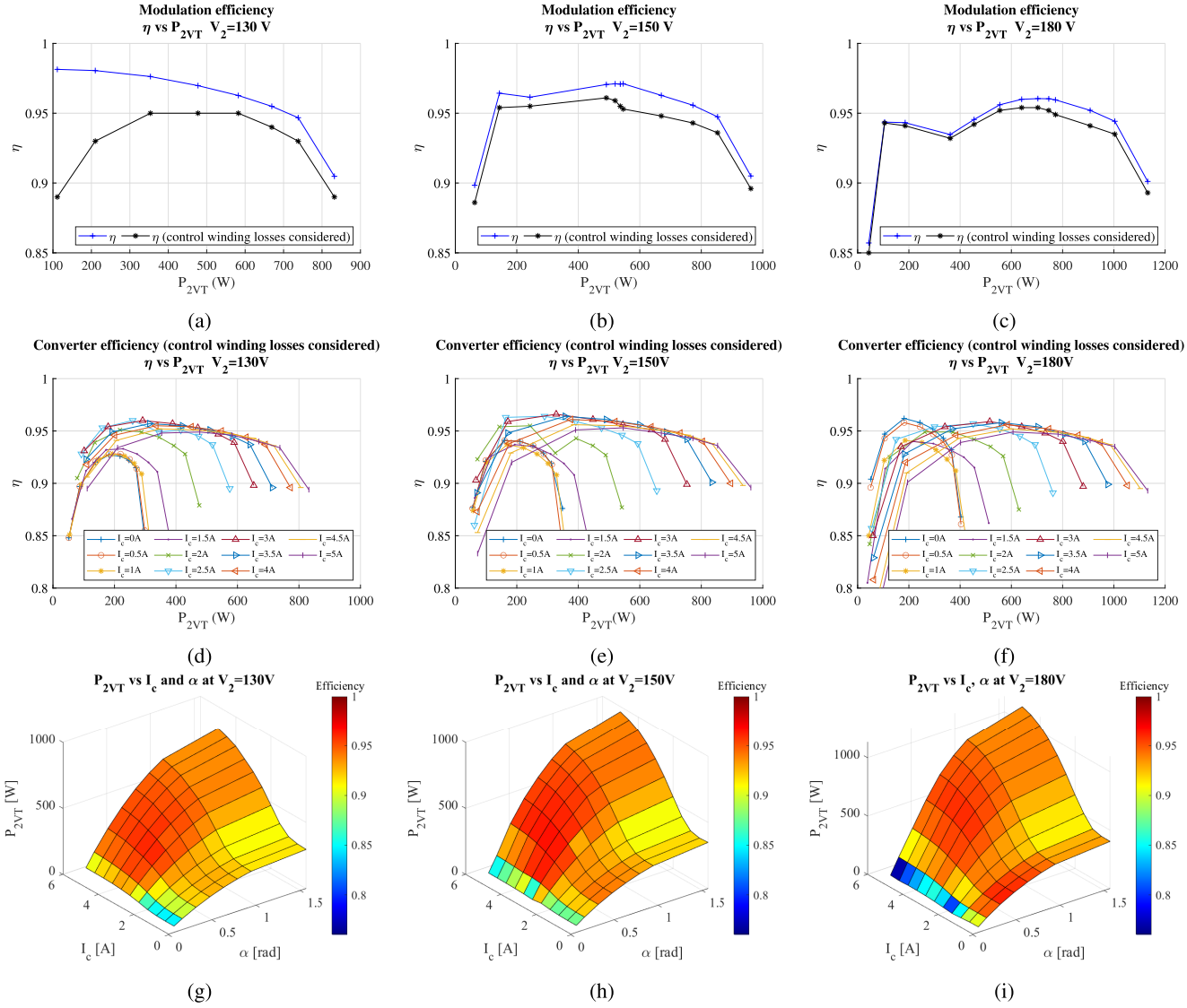

FIGURE 29. DAB+VT Converter efficiency for V_2 =130 V, 150 V, 180 V: (a) -(c) impact of the control winding operation on the modulation strategy efficiency, (d)-(f) I_c sweep, (g)-(i) converter power surface and efficiency color map.

kept, see Fig. 25. This condition ensures that both converters have the same power capability, thereby facilitating a comprehensive assessment between them.

Figs. 26 - 28 compare the theoretical effective currents in the VT against the experimental results, considering the same control parameters, α and I_c, as determined by the modulation algorithm. Additionally, the ideal reference DAB currents are plotted as a comparison element between a conventional DAB implementation and the DAB+VT solution.

The results demonstrate the reduction of the effective currents achieved through the adopted modulation technique when compared to the reference DAB, particularly under low load and mismatched voltage conditions (see, Figs. 26c, 26d, 27c, 27d). However, it is important to note that attained power levels are lower for high V_2 and α values, attributed to large magnetic flux variations in the VT resulting from these operating conditions. Additionally, for $\alpha > \pi/4$, the presence of high effective currents in relation to the converter's power translate into higher conduction losses, decreasing its efficiency.

Furthermore, for $V_1 \approx V_2/n_{eq}$, the currents of the DAB+VT and the reference DAB match, indicating the low negative impact of the reduced parallel-series inductance ratio of the VT in the converter topology, see in Figs. 28c, 28d.

F. CONVERTER'S EFFICIENCY

The primary goal of incorporating a VT into a DAB is to minimize power losses under wide voltage and load conditions. In particular, for light-loads, increasing the series inductance, L_a, effectively reduces the circulating currents in the converter, achieving a minimum at $V_1 \approx V_2/n_{eq}$. Ideally, this condition results in ZVS for both bridges,

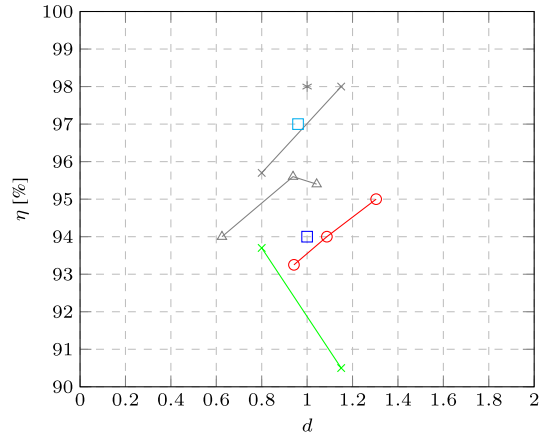

(a) Efficiency at 10 % of maximum load

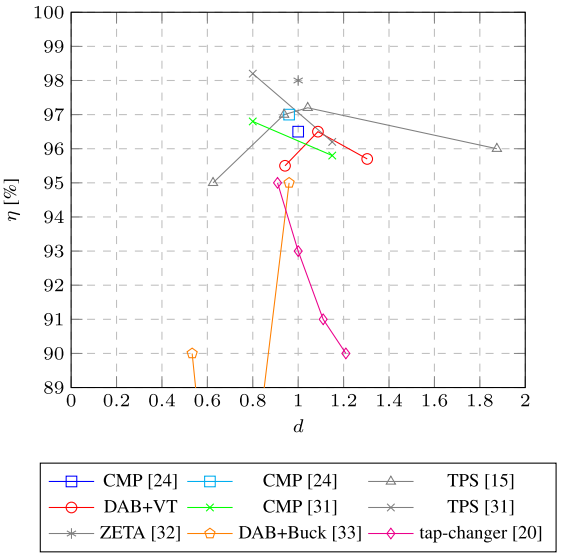

(b) Efficiency at 20 % of maximum load

FIGURE 30. DAB+VT performance comparison under light-load and wide voltage operation.

leading to improved efficiency compared to the traditional implementation. However, the incorporation of the VT control winding incurs additional conduction losses during operation. Furthermore, the effects of the MOSFETs' and the transformer's capacitances can limit the achievement of soft commutation at light-loads, despite achieving matched voltage conditions through the controllable transformer.

Figs. 29a-29c illustrate the impact of the control winding operation on the efficiency of modulation strategy, showing significant losses for $V_2 = 130$ V, where I_c is set to 5 A to achieve a unitary value of the primary referred DC voltage gain, d. While increasing N_c reduces the control winding losses, it is essential to take into account the resultant higher inter-winding capacitance, aiming to minimize its impact on the converter's ZVS region.

Figs.29d - 29f show that slight deviations in the control current obtained by the modulation strategy can enhance the efficiency by achieving the actual conditions for ZVS or quasi-ZVS. As such, efficiencies $\eta > 90\%$ across wide load and voltage conditions were obtained by the implementation of the VT.

Finally, Figs. 29g-29i demonstrate that $\alpha > \pi/4$ results in a generalized drop in converter efficiency. Therefore, maintaining $\alpha < \pi/4$ is recommended, not only to reduce $B_{AC_{Ca.bpk}}$ and avoid high variations in the VT parameters (increased L_a), but also to maintain the DAB operating close to its power quasi-linear region limiting the converter's conduction losses.

G. DAB+VT PERFORMANCE

The DAB+VT is assessed by comparing it with state-of-the-art DAB converters operating under similar power ranges and conditions, with particular focus on advanced modulation techniques implementations. While the efficiency of a power converter is affected by factors beyond modulation strategy (e.g., switching device, switching frequency), the presented results offer a preliminary evaluation within the constraints of performing a comparison under non-identical conditions. Nonetheless, the analysis provides valuable insights into the observed differences.

To evaluate light-load operation consistently, the efficiency is compared at 10% and 20% of the maximum load, as defined by (1) for $\alpha = \pi/2$. Furthermore, wide-voltage conditions are rated by the variation of parameter d, defined by (2).

The results are illustrated in Fig. 30, where implementations using CPM are represented in color and considered comparable to the presented solution in this paper. Conversely, studies employing complex modulation techniques are displayed in gray, indicating the potential improvements that can be achieved by incorporating these techniques into the DAB+VT.

As seen, the highest efficiencies are achieved when the converter operates near matched voltage conditions ($d = 1$). In [31] (asterisk marker), the authors obtained 98% efficiency through complex modulation (Z mode), although at a high computational cost. Meanwhile, in [24] (square marker), the authors achieved efficiencies around 97% using CPM along with reduced magnetzing inductance. However, for operation under wide voltage and light-load conditions, the implementation of TPS modulation is necessary. This is evidenced by studies in [15] and [31] ($\times$ and triangle markers, respectively).

In this context, Fig. 30a shows that the DAB+VT (circle marker) outperforms the conventional CMP implementations at 10% of the maximum load under wide-voltage conditions, achieving comparable efficiencies to the TPS implementation in [15] (triangle marker). As depicted in Fig. 30b, at 20% of the load, the difference between the different modulation techniques diminishes, however, it is important to notice how DAB + VT presents a superior performance when compared to DAB with a transformer tap changer mechanism in [33] (pentagon marker) and the cascaded DAB plus buck converter in [20] (diamond marker).

The remarkable results presented by the authors in [15] deserve attention, as they are achieved in part by adopting

a reduced magnetzing inductance, which extends the ZVS region under light-load conditions. This approach aligns with the operational characteristics of the DAB+VT converter. Importantly, the adoption of complex modulation techniques is not mutually exclusive with the approach in this study, as these techniques can be combined to broaden the converter's operating capabilities.

VI. CONCLUSION AND FUTURE WORK

This study validates the concept of the VT in DAB converters, which provides an additional degree of freedom to the converter topology operation by controlling its equivalent turns ratio n_{eq}. The VT offers several benefits, including a reduction in the effective currents under wide voltage and load conditions, improved efficiency at light loads, and an extension of the ZVS region under current-based conditions.

The requirement to maintain the core AC flux density of the VT under small signal conditions results in a decreased converter power density. Nevertheless, using alternative premagnetisation methods to control the reluctance of the core, and improved core shapes can lead to a more compact VT solution. In general, the DAB+VT solution can be comparable in terms of power density to those DAB systems that require a series inductor, typically implemented at medium-low power levels.

To fully exploit the advantages of the VT, it is necessary to carefully select the minimum parallel-series inductance ratio K to achieve a large gain G and an extended ZVS region while limiting the circulating currents. Furthermore, an optimisation procedure is required to reduce the conduction losses associated with the operation of the control winding while maintaining a low winding capacitance to reduce its impact on the attainment of soft commutation at light loads.

Although the use of the VT in conjunction with the proposed modulation technique achieves minimum effective currents at light loads, it does not necessarily result in maximum efficiencies. Therefore, energy-based conditions must be considered to achieve ZVS or quasi-ZVS commutation under such load conditions. However, on the basis of the efficiency measurements of the converter, this is feasible.

Moreover, the utilization of the VT can be combined with more sophisticated modulation strategies, such as TPS and DPS, to enhance the DAB converter's performance across a wider range of voltage operating conditions beyond what can be achieved by implementing a single technique.

APPENDIX A
VT FLUX DENSITY DERIVATION

According to the winding configuration of the transformer, the secondary voltage is defined as follows:

$$v_{ac2} = v_{w_{s1}} + v_{w_{s2}} \tag{25}$$

Assuming a thigh coupling between the windings w_p and w_{s1}, the voltage of this winding is given by the following expression:

$$v_{w_{s1}} \approx \frac{N_{s1} v_{ac1}}{N_p} \tag{26}$$

Therefore, the voltage $v_{w_{s2}}$ is obtained as:

$$v_{w_{s2}} \approx v_{ac2} - \frac{N_{s1} v_{ac1}}{N_p} \tag{27}$$

Figure 31 depicts the DAB+VT typical voltage and magnetic flux waveforms.

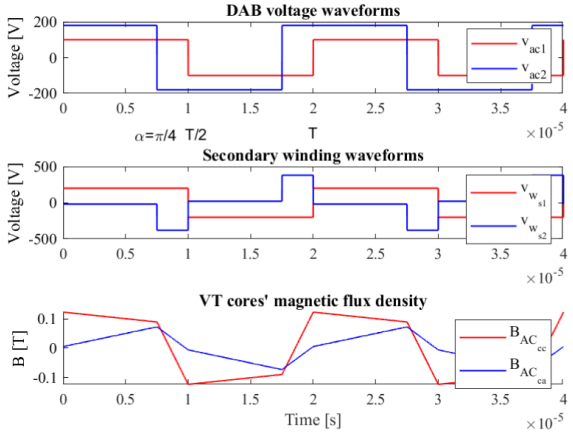

FIGURE 31. DAB+VT typical voltage and flux waveforms.

As seen, the $v_{w_{s2}}$ can be described by the following piecewise function:

$$v_{w_{s2}}(t) = \begin{cases} V_2 - V_1 \frac{N_{s1}}{N_p} & if\, 0 \le t \le \frac{\alpha T}{2\pi} \\ -V_2 - V_1 \frac{N_{s1}}{N_p} & if\, \frac{\alpha T}{2\pi} < t \le \frac{T}{2} \\ -V_2 + V_1 \frac{N_{s1}}{N_p} & if\, \frac{T}{2} < t \le \frac{T}{2} + \frac{\alpha T}{2\pi} \\ V_2 - V_1 \frac{N_{s1}}{N_p} & if\, \frac{T}{2} + \frac{\alpha T}{2\pi} < t \le T \end{cases} \tag{28}$$

Thus, the magnetic flux through this winding is defined as:

$$\phi_{AC_2}(t) = \int \frac{v_{w_{s2}}(t)}{N_{s2}}\, dt + C \tag{29}$$

where,

$$\frac{1}{T}\int_0^T \phi_{AC_2}(t)\, dt = 0 \tag{30}$$

Hence, the magnetic flux density of the core-set c is given by:

$$B_{AC_{Cc}} = \frac{\phi_{AC_2}}{A_c} \tag{31}$$

Similarly, the AC flux density of the core-sets a and b is obtained as follows:

$$B_{AC_{Ca,b}} = \frac{\phi_{AC_1} + \phi_{AC_2}}{2A_c} \tag{32}$$

where

$$\phi_{AC_1}(t) = \int \frac{v_{ac1(t)}}{N_p}\, dt + C \tag{33}$$

$$\frac{1}{T}\int_0^T \phi_{AC_1}(t)\, dt = 0 \tag{34}$$

APPENDIX B
DAB VT DESIGN STEPS

While a comprehensive explanation of the working principle of the VT can be found in [22], the distribution of the magnetic flux density in the cores is influenced by the specific converter topology. Consequently, a generalised procedure for designing the transformer within a DAB converter is provided as follows:

TABLE 1. VT design procedure.

Step	Action
01	Specify V_1, V_2, f_s, P_{2VT}, $min(n_{eq})$, $Max(n_{eq})$ and allowed control winding losses
02	Calculate the required equivalent turns ratio gain G
03	Estimate a total variation of the reluctance R_{v_U}
04	Obtain K and N_{sr} from [22, Figs 14-15]
05	Considering P_{2VT} and $min(n_{eq})$ determine $min(L_a)$
06	Select the core size and material based on a "non-saturated thermal design" approach for $I_c = 0$ refer to [34]
07	Solve N_p from expressions (15) and (16) while keeping the small-signal conditions for the flux density
08	Solve N_{s1} from [22, equation (19)]
09	Calculate/simulate $min(L_a)$ and adjust the air-gap if required
10	If the air-gap was adjusted go to step 03, else go to step 11
11	Calculate the number of turns a wire specifications of the control winding according to max allowed losses

REFERENCES

[1] R. W. De Doncker, D. M. Divan, and M. H. Kheraluwala, "A three-phase soft-switched high power density DC/DC converter for high power applications," in *Proc. Conf. Rec. IEEE Ind. Appl. Soc. Annu. Meeting*, 1988, pp. 796–805.

[2] F. Krismer and J. W. Kolar, "Closed form solution for minimum conduction loss modulation of DAB converters," *IEEE Trans. Power Electron.*, vol. 27, no. 1, pp. 174–188, Jan. 2012.

[3] R. W. A. A. De Doncker, D. M. Divan, and M. H. Kheraluwala, "A three-phase soft-switched high-power-density DC/DC converter for high-power applications," *IEEE Trans. Ind. Appl.*, vol. 27, no. 1, pp. 63–73, 1991.

[4] J. Hiltunen, V. Väisänen, R. Juntunen, and P. Silventoinen, "Variable-frequency phase shift modulation of a dual active bridge converter," *IEEE Trans. Power Electron.*, vol. 30, no. 12, pp. 7138–7148, Dec. 2015.

[5] Q. Gu, L. Yuan, J. Nie, J. Sun, and Z. Zhao, "Current stress minimization of dual-active-bridge DC–DC converter within the whole operating range," *IEEE J. Emerg. Sel. Topics Power Electron.*, vol. 7, no. 1, pp. 129–142, Mar. 2019.

[6] H. Yu, L. Hang, X. Zheng, Z. He, Y. He, L. Shen, C. Shao, P. Zeng, Q. Wu, X. Yang, and H. Tao, "Globally unified ZVS and quasi-optimal minimum conduction loss modulation of DAB converters," *IEEE Trans. Transport. Electrific.*, vol. 8, no. 3, pp. 3989–4000, Sep. 2022.

[7] N. Noroozi, A. Poorfakhraei, O. Zayed, A. Elezab, N. Keshmiri, M. Narimani, and A. Emadi, "RMS current minimization in a SiC-based dual active bridge converter using triple-phase-shift modulation," *IEEE Trans. Ind. Electron.*, vol. 70, no. 7, pp. 7173–7182, Jul. 2023.

[8] L. Zhou, Y. Gao, H. Ma, and P. T. Krein, "Wide-load range multiobjective efficiency optimization produces closed-form control solutions for dual active bridge converter," *IEEE Trans. Power Electron.*, vol. 36, no. 8, pp. 8612–8616, Aug. 2021.

[9] L. Li, G. Xu, W. Xiong, D. Liu, and M. Su, "An optimized DPS control for dual-active-bridge converters to secure full-load-range ZVS with low current stress," *IEEE Trans. Transport. Electrific.*, vol. 8, no. 1, pp. 1389–1400, Mar. 2022.

[10] L. Gong, X. Jin, J. Xu, Z. Deng, H. Li, T. B. Soeiro, and Y. Wang, "A dynamic ZVS-guaranteed and seamless-mode-transition modulation scheme for the DAB converter that maximizes the ZVS range and lowers the inductor RMS current," *IEEE Trans. Power Electron.*, vol. 37, no. 11, pp. 13119–13134, Nov. 2022.

[11] J. Li, Q. Luo, D. Mou, Y. Wei, and X. Zhang, "Comprehensive optimization modulation scheme of low current level and wide ZVS range for dual active bridge converter with dead-zone control," *IEEE Trans. Power Electron.*, vol. 37, no. 3, pp. 2731–2748, Mar. 2022.

[12] S. Shao, M. Jiang, W. Ye, Y. Li, J. Zhang, and K. Sheng, "Optimal phase-shift control to minimize reactive power for a dual active bridge DC–DC converter," *IEEE Trans. Power Electron.*, vol. 34, no. 10, pp. 10193–10205, Oct. 2019.

[13] Y. Yan, H. Bai, A. Foote, and W. Wang, "Securing full-power-range zero-voltage switching in both steady-state and transient operations for a dual-active-bridge-based bidirectional electric vehicle charger," *IEEE Trans. Power Electron.*, vol. 35, no. 7, pp. 7506–7519, Jul. 2020.

[14] F. Lin, X. Zhang, X. Li, C. Sun, W. Cai, and Z. Zhang, "Automatic triple phase-shift modulation for DAB converter with minimized power loss," *IEEE Trans. Ind. Appl.*, vol. 58, no. 3, pp. 3840–3851, May 2022.

[15] D. Chen, J. Deng, M. Li, and Z. Wang, "Simplified closed-form optimized trajectories control for a dual active bridge converter with ZVS implementation over whole domain," *IEEE Trans. Power Electron.*, vol. 37, no. 10, pp. 11749–11761, Oct. 2022.

[16] L. Deng, G. Zhou, Q. Bi, and N. Xu, "Online reactive power minimization and soft switching algorithm for triple-phase-shift modulated dual active bridge converter," *IEEE Trans. Ind. Electron.*, vol. 70, no. 3, pp. 2543–2555, Mar. 2023.

[17] S. Pistollato, N. Zanatta, T. Caldognetto, and P. Mattavelli, "A low complexity algorithm for efficiency optimization of dual active bridge converters," *IEEE Open J. Power Electron.*, vol. 2, pp. 18–32, 2021.

[18] S. Saeed, J. Garcia, and R. Georgious, "Dual-active-bridge isolated DC–DC converter with variable inductor for wide load range operation," *IEEE Trans. Power Electron.*, vol. 36, no. 7, pp. 8028–8043, Jul. 2021.

[19] X. Chen, G. Xu, H. Han, Y. Sun, Y. Liu, and M. Su, "Modulated coupled inductor for input-serial-output-parallel dual-active-bridge converter," *IEEE Trans. Ind. Electron.*, vol. 69, no. 6, pp. 6450–6455, Jun. 2022.

[20] A. Jafari, M. S. Nikoo, F. Karakaya, and E. Matioli, "Enhanced DAB for efficiency preservation using adjustable-tap high-frequency transformer," *IEEE Trans. Power Electron.*, vol. 35, no. 7, pp. 6673–6677, Jul. 2020.

[21] S. Taraborrelli, R. Spenke, and R. W. De Doncker, "Bidirectional dual active bridge converter using a tap changer for extended voltage ranges," in *Proc. 18th Eur. Conf. Power Electron. Appl. (EPE ECCE Europe)*, Sep. 2016, pp. 1–10.

[22] C. Suarez, D. B. Cobaleda, W. Martinez, and K. Leuven, "Magnetically controlled transformer with variable turns ratio and low series-inductance: Analysis and implementation towards its application in SMPS," *IEEE Trans. Power Electron.*, early access, Aug. 1, 2023, doi: 10.1109/TPEL.2023.3300583.

[23] J. Riedel, D. G. Holmes, B. P. McGrath, and C. Teixeira, "Maintaining continuous ZVS operation of a dual active bridge by reduced coupling transformers," *IEEE Trans. Ind. Electron.*, vol. 65, no. 12, pp. 9438–9448, Dec. 2018.

[24] X. Chen, G. Xu, H. Han, D. Liu, Y. Sun, and M. Su, "Light-load efficiency enhancement of high-frequency dual-active-bridge converter under SPS control," *IEEE Trans. Ind. Electron.*, vol. 68, no. 12, pp. 12941–12946, Dec. 2021.

[25] M. N. Kheraluwala, R. W. Gascoigne, D. M. Divan, and E. D. Baumann, "Performance characterization of a high-power dual active bridge DC-to-DC converter," *IEEE Trans. Ind. Appl.*, vol. 28, no. 6, pp. 1294–1301, Nov./Dec. 1992.

[26] G. Xu, L. Li, X. Chen, W. Xiong, X. Liang, and M. Su, "Decoupled EPS control utilizing magnetizing current to achieve full load range ZVS for dual active bridge converters," *IEEE Trans. Ind. Electron.*, vol. 69, no. 5, pp. 4801–4813, May 2022.

[27] S. Yin, S. Debnath, R. Wojda, P. Marthi, and M. Saeedifard, "Impact of the transformer magnetizing inductance on the performance of the dual-active bridge converter," in *Proc. IEEE 22nd Workshop Control Model. Power Electron. (COMPEL)*, Nov. 2021, pp. 1–7.

[28] J. Everts, "Closed-form solution for efficient ZVS modulation of DAB converters," *IEEE Trans. Power Electron.*, vol. 32, no. 10, pp. 7561–7576, Oct. 2017.
[29] J. M. Alonso, M. Perdigão, M. A. D. Costa, S. Zhang, and Y. Wang, "Analysis and experimentation of the quad-U variable inductor for power electronics applications," *IET Power Electron.*, vol. 11, no. 14, pp. 2330–2337, Nov. 2018, doi: 10.1049/iet-pel.2018.5126.
[30] J. M. Alonso, G. Martínez, M. Perdigão, M. R. Cosetin, and R. N. do Prado, "A systematic approach to modeling complex magnetic devices using SPICE: Application to variable inductors," *IEEE Trans. Power Electron.*, vol. 31, no. 11, pp. 7735–7746, Nov. 2016.
[31] A. Tong, L. Hang, G. Li, X. Jiang, and S. Gao, "Modeling and analysis of a dual-active-bridge-isolated bidirectional DC/DC converter to minimize RMS current with whole operating range," *IEEE Trans. Power Electron.*, vol. 33, no. 6, pp. 5302–5316, Jun. 2018.
[32] Z. Ye, C. Li, J. Liu, and Z. Zheng, "Towards full range zero-voltage switching of DAB converters: An improved multi-mode modulation at light loads under close-to-unity voltage ratio," *IEEE Trans. Power Electron.*, vol. 38, no. 6, pp. 6912–6917, Jun. 2023.
[33] Z. Lu, G. Xu, W. Xiong, Y. Sun, and M. Su, "A quasi-two-stage isolated bidirectional buck-DAB converter for wide input voltage range," *IEEE Trans. Power Electron.*, vol. 38, no. 2, pp. 1384–1390, Feb. 2023.
[34] V. Valchev and A. Van den Bossche, *Inductors and Transformers for Power Electronics*. Boca Raton, FL, USA: CRC Press,Feb. 2005, p. 480.

CAMILO SUAREZ BUITRAGO was born in Tunja, Boyacá, Colombia. He received the B.Eng. degree in electronics engineering from Universidad Nacional de Colombia, Bogotá, Colombia, in 2011, and the M.Sc. degree in electrical engineering from Universidade Estaudal Paulista (UNESP), Ilha Solteira, São Paulo, Brazil, in 2017. He is currently pursuing the Ph.D. degree in engineering technology with KU Leuven, Leuven, Belgium.

His research interest includes the development of high-frequency high-power isolated dc–dc converters for EV chargers.

DIEGO BERNAL COBALEDA (Student Member, IEEE) was born in Bucaramanga, Santander, Colombia, in 1990. He received the B.Eng. and M.Sc. degrees in electronic engineering from Pontificia Universidad Javeriana, Bogotá, Colombia, in 2015 and 2017, respectively. He is currently pursuing the Ph.D. degree in engineering with KU Leuven, Leuven, Belgium.

His current research is focused on power static converters for more electric aircraft applications toward improving power density in the low-voltage dc–dc grids of commercial shuttles. His research interests include power converters, magnetic components, energy systems, and the environmental impact of transportation systems.

WILMAR MARTINEZ (Senior Member, IEEE) received the B.S. degree in electronics engineering and the M.Sc. degree in electrical engineering from Universidad Nacional de Colombia, Bogotá, Colombia, in 2011 and 2013, respectively, and the Ph.D. degree in electronic function and system engineering from Shimane University, Matsue, Japan, in 2016.

He was a Postdoctoral Researcher with the Toyota Technological Institute, Japan, in 2016, and Aalto University, Finland, in 2017. In 2018, he joined KU Leuven, Leuven, Belgium, as an Assistant Professor with the Department of Electrical Engineering, where he has been an Associate Professor, since 2023. Additionally, he serves as a Coordinator with the Research Line Power Electronics, EnergyVille, Genk, Belgium. His research interests include a wide range of areas of power conversion for energy and transportation systems, battery charging infrastructure, and electric powertrain development through the multiobjective optimization of power converters, evaluation of iron losses of magnetic materials, and study of SiC and GaN switching devices.